17. Fluoxetine is an SSRI. Imipramine is a TCA that blocks the reuptake of both 5-HT and NA. Desipramine is a TCA that selectively blocks NA reuptake. Haloperidol is a neuroleptic devoid of antidepressant activity.
18. P. A. Sargent *et al.*, *Arch. Gen. Psychiatry* **57**, 174 (2000).
19. C. Gross *et al.*, *Nature* **416**, 396 (2002).
20. E. Tada, J. M. Parent, D. H. Lowenstein, J. R. Fike, *Neuroscience* **99**, 33 (2000).
21. See materials and methods on *Science* Online.
22. R. Nagai, S. Tsunoda, Y. Hori, H. Asada, *Surg. Neurol.* **53**, 503 (2000).
23. L. Santarelli *et al.*, data not shown.
24. G. Griebel *et al.*, *Proc. Natl. Acad. Sci. U.S.A.* **99**, 6370 (2002).
25. J. E. LeDoux, P. Cicchetti, A. Xagoraris, L. M. Romanski, *J. Neurosci.* **10**, 1062 (1990).
26. J. M. Gorman, *J. Clin. Psychiatry* **63**, 17 (2002).
27. P. L. Delgado *et al.*, *Biol. Psychiatry* **46**, 212 (1999).
28. M. E. Page, M. J. Detke, A. Dalvi, L. G. Kirby, I. Lucki, *Psychopharmacology* **147**, 162 (1999).
29. S. Ramboz *et al.*, *Proc. Natl. Acad. Sci. U.S.A.* **95**, 14476 (1998).
30. N. McNaughton, *Pharmacol. Biochem. Behav.* **56**, 603 (1997).
31. H. Eichenbaum, *Curr. Biol.* **9**, R482 (1999).
32. J. A. Gray, N. MaNaughton, *The Neuropsychology of Anxiety* (Oxford Univ. Press, Oxford, ed. 2, 2000).
33. G. Kempermann, *Bipolar Disord.* **4**, 17 (2002).
34. J. Menard, D. Treit, *Behav. Pharmacol.* **9**, 93 (1998).
35. S. E. File, P. J. Kenny, S. Cheeta, *Pharmacol. Biochem. Behav.* **66**, 65 (2000).
36. J. Menard, D. Treit, *Brain Res.* **888**, 163 (2001).
37. R. M. Deacon, D. M. Bannerman, J. N. Rawlins, *Behav. Neurosci.* **116**, 494 (2002).
38. A. Degroot, D. Treit, *Brain Res.* **949**, 60 (2002).
39. D. M. Bannerman *et al.*, *Behav. Neurosci.* **116**, 884 (2002).
40. Y. Shirayama, A. Chen, S. Nakagawa, D. Russell, R. Duman, *J. Neurosci.* **22**, 3251 (2002).
41. G. J. Moore *et al.*, *Lancet* **356**, 1241 (2000).
42. We thank J. Malberg, A. Dhilla, and G. Johnson for their help; W. Dauer, M. Groszer, E. Kandel, P. Rakic, G. Fishbach, F. Gage, A. Kriegstein, and J. Goldman for comments and suggestions; and N. Annenberg for his support. Supported by grants from the National Institute on Drug Abuse (R.H.), National Institute of Mental Health (R.H.), and National Alliance for Research on Schizophrenia and Depression (R.H. and L.S.).

Supporting Online Material

www.sciencemag.org/cgi/content/full/301/5634/805/DC1
Materials and Methods
Figs. S1 to S3
References

11 February 2003; accepted 27 June 2003

REPORTS

An All-Optical Quantum Gate in a Semiconductor Quantum Dot

Xiaoqin Li,[1] Yanwen Wu,[1] Duncan Steel,[1]* D. Gammon,[2] T. H. Stievater,[2] D. S. Katzer,[2] D. Park,[2] C. Piermarocchi,[3] L. J. Sham[4]

We report coherent optical control of a biexciton (two electron-hole pairs), confined in a single quantum dot, that shows coherent oscillations similar to the excited-state Rabi flopping in an isolated atom. The pulse control of the biexciton dynamics, combined with previously demonstrated control of the single-exciton Rabi rotation, serves as the physical basis for a two-bit conditional quantum logic gate. The truth table of the gate shows the features of an all-optical quantum gate with interacting yet distinguishable excitons as qubits. Evaluation of the fidelity yields a value of 0.7 for the gate operation. Such experimental capability is essential to a scheme for scalable quantum computation by means of the optical control of spin qubits in dots.

The rapid evolution of quantum dot (QD) studies has opened up the possibility of building devices that reveal both classical and quantum features. In particular, biexciton transitions in QDs have been proposed as the physical realization of universal quantum logic gates (*1*–*3*). In a single QD, quantum confinement greatly enhances the higher order Coulomb interaction, leading to the formation of a bound state of two orthogonally polarized excitons. The excitation of one exciton affects the resonant energy of the other, which corresponds to the characteristic conditional quantum dynamics that are needed for quantum computing.

[1]Frontiers in Optical Coherent and Ultrafast Science (FOCUS), Harrison M. Randall Laboratory of Physics, The University of Michigan, Ann Arbor, Michigan 48109–1120, USA. [2]Naval Research Laboratory, Washington, DC 20375–5347, USA. [3]Department of Physics and Astronomy, Michigan State University, East Lansing, MI 48824–2320, USA. [4]Department of Physics, The University of California, San Diego, La Jolla, CA 92093–0319, USA.

*To whom correspondence should be addressed. E-mail: dst@umich.edu

Fig. 1, A and B, shows the mapping from the single-particle picture of the two exciton transitions in a single QD to the excitation-level diagram. This simplest two-bit system involves the crystal ground state ($|00\rangle$), two distinguishable excitonic states with orthogonal polarizations ($|01\rangle$ and $|10\rangle$), and the biexciton state ($|11\rangle$), where the value 0 (or 1) represents the absence (or presence) of an exciton. In a controlled rotation (CROT) gate, the target bit (the second bit) is rotated through π (i.e., from state 0 to 1 or vice versa) if and only if the control bit (the first bit) is 1. The unitary transformation matrix of the CROT shown in Fig. 1C operates on the input wave function defined in the computational basis and yields the output wave function. The CROT gate is equivalent to the standard controlled-NOT (CNOT) gate, despite the slight difference in the minus-sign placement in their matrix representations (*4*). Unitary rotations like the CROT are much easier to realize than the CNOT operations (*4*, *5*).

We demonstrated Rabi oscillations between the exciton and biexciton states that are similar to the excited-state Rabi oscillations observed in atomic systems. This work builds on earlier demonstrations of the ground-state-to-exciton Rabi oscillations in QDs (*6*–*9*). The result is important in that the π pulse in this experiment plays a critical role in quantum information processing. It transforms a factorizable state into an entangled state: $|00\rangle + |10\rangle \rightarrow |00\rangle + |11\rangle$. It can also be used as the operational pulse for the CROT. When we combine this result with the exciton Rabi oscillations, the truth table of a CROT gate can be mapped out in this two-bit system. The performance of the gate is

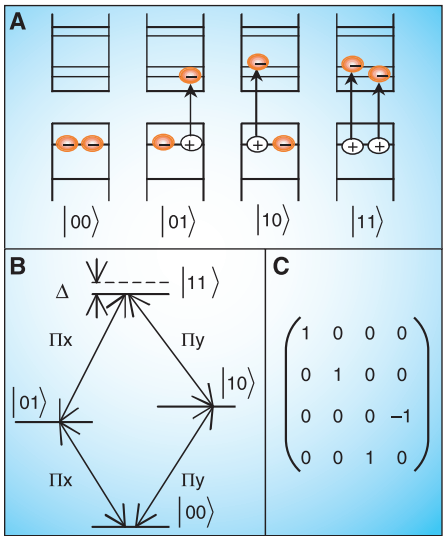

Fig. 1. (**A**) Two exciton transitions in a single QD. (**B**) Excitation-level diagram, where $|00\rangle$, $|01\rangle$ and $|10\rangle$, and $|11\rangle$ denote the ground state, the excitons, and the biexciton, respectively. The optical selection rules for various transitions are labeled. Π_x and Π_y indicate orthogonally and linearly polarized lights. Δ represents the binding energy. (**C**) The transformation matrix for a CROT gate.

limited by the short population relaxation times of dipole-allowed transitions and the long operational pulses used to avoid exciting nearby states outside the computational basis.

The current system is clearly not scalable beyond two qubits, but serves instead as a model for studies that may lead to more complex scalable systems (*10*, *11*). Any quantum algorithm requiring only two qubits, such as the Deutsch-Jozsa algorithm, can be realized in the current biexciton system, in which necessary quantum transformations are decomposed into single-bit rotations and the two-bit CROT (*4*).

QDs are naturally formed in a thin (4.2 nm) GaAs layer grown between two 25-nm $Al_{0.3}Ga_{0.7}As$ barriers and are probed through submicron apertures at 6 K (*12*, *13*). The exciton states are excited with linearly polarized light, and the biexciton is excited by the collinear polarization rules (Fig. 1B). These selection rules result from the tendency of the QD islands to elongate along the [$\bar{1}$10] crystal axis and have been verified in previous studies (*14*). The fine structure splitting between the two orthogonally polarized excitons is on the order of tens of μeV.

Biexcitons, together with the related excitons, have been characterized in naturally formed QDs with nonlinear optical spectroscopy in the frequency domain (*15*). Our work extends that study with coherent, transient, differential transmission (DT) measurements (*16*). A DT experiment mapped out the single excitonic transitions under a small aperture (Fig. 2A). The data were taken by fixing the delay (τ) between the pump (E_1, ω_1, where E is the electric field and ω is the laser frequency) and the probe (E_2, $\omega_2 = \omega_1$) near zero and scanning the frequency of the laser. The resonances were broadened by the laser bandwidth (~0.4 meV) (supporting online text). Experiments designed to study the biexciton require a two-color excitation scheme. The first laser, producing a strong pre-pulse (E_{pre}), was tuned to an exciton transition. It prepared the system by driving it from state $|00\rangle$ to $|10\rangle$, for example. The second laser, in the usual pump-and-probe geometry, then manipulated the state and probed the result. When the pump and probe beams were scanned in frequency with τ fixed near zero, a peak at the lower energy end of the spectrum appeared (Fig. 2C), which corresponds to the biexciton transition related to the exciton that was excited by the pre-pulse. The energy difference, ~3.5 meV, between the biexciton and the associated exciton is the biexciton binding energy, which is considerably higher than that reported in higher dimensional semiconductor structures (*15*).

Rabi oscillations are well-understood phenomena in two-level spin and atomic systems. Under a strong, resonant, coherent excitation field, the population of the excited state goes through an oscillation as a function of pulse area, which is defined as $\Theta(t) = [(\boldsymbol{\mu}_{eg} \cdot \hat{\varepsilon}_1)/\hbar]\int_{-\infty}^{t} E_1(t')dt'$, where Θ is the pulse area, t is time, $\boldsymbol{\mu}_{eg}$ is the electric dipole moment of the transition, ε is the electric field polarization vector, and, $\hbar$ is Planck's constant h divided by 2π. The analytical solution to the simplest two-level model with no dephasing shows that the excited-state population evolves in time as $\sin^2[\Theta(t)/2]$.

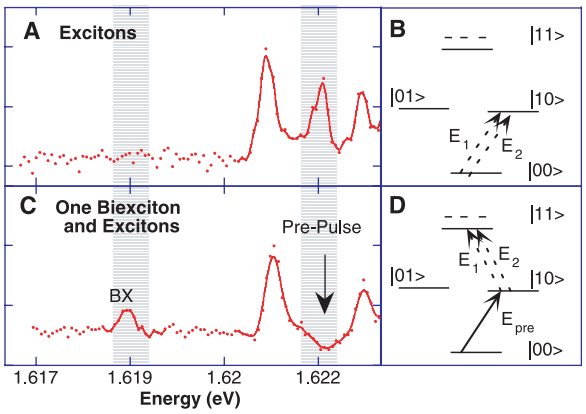

Fig. 2. (**A** and **B**) The spectrum and experimental configuration of DT that mapped out the excitons. (**C** and **D**) The DT spectrum and experimental configuration with a pre-pulse tuned to one exciton transition and the biexciton state appearing at the lower energy end. Dotted arrows indicate the laser is scanned in frequency; solid arrows indicate fixed frequency. Shaded areas mark areas of interest. BX, biexciton.

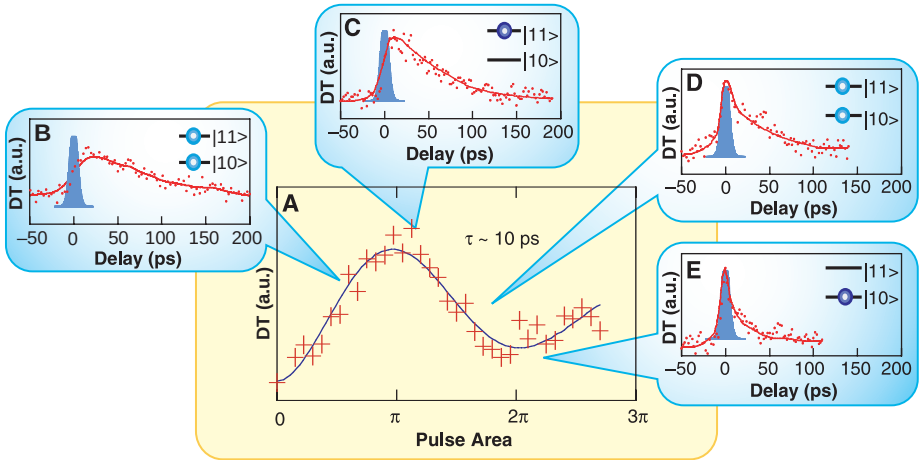

Fig. 3. Biexciton Rabi oscillations. (**A**) Measured DT versus pump-field amplitude at a fixed-delay position (τ ~ 10 ps). The solid line is a sine-squared function with exponentially decaying amplitudes fit to the data. (**B** to **E**) DT versus probe delay at fixed pump powers. The target states that follow the pump pulse (shaded area) are shown in the upper right, where the circles represent the exciton population. The solid lines are guides to the eye. The peak intensity corresponding to the 2π pulse is ~32 kW/cm^2.

The experimental configuration for the biexciton Rabi-oscillation experiment was similar to that shown in Fig. 2D, except that the probe polarization was chosen to be orthogonal to the pump to probe the $|11\rangle \rightarrow |01\rangle$ transition and to monitor the population of state $|11\rangle$. A polarizer was placed in front of the detector to avoid excess noise caused by the strong pump field. The delay between the pump and the probe was fixed at τ ~ 10 ps. As the pump power, i.e., the pulse area, varied, one complete oscillation was observed (Fig. 3A) with the peak of the oscillation corresponding to a pulse area of ~π and the trough corresponding to ~2π. After estimating the electric field amplitude at the QD that corresponds to the 2π pulse, we extracted the dipole moment, ~77 Debye, which is comparable to the exciton dipole moments previously reported (*17*).

The amplitude of the Rabi oscillations decays as seen earlier in the exciton Rabi oscillations, because of an increase in the population decay rate (*6*). The physical origin for an increased decay rate at higher pump power is a higher scattering rate experienced by the resonantly excited excitons and biexcitons from the nearly degenerate delocalized states. Strong evidence of the existence of such delocalized states has been observed in ensemble studies.

Biexciton Rabi oscillations could also be observed as a function of pulse delay at fixed pump powers (Fig. 3, B to E). The target quantum states that followed the pump pulse were $1/\sqrt{2}(|10\rangle - |11\rangle)$, $-|11\rangle$, $-1/\sqrt{2}(|10\rangle + |11\rangle)$, and $-|10\rangle$, from left to right. The post–pump-pulse time evolution was simply due to the population relaxation. When the pulse area exceeded π, stimulated emission began. This was most clearly demonstrated in the case of a 2π pulse, where the maximum population was excited and then immediately switched back down.

An important achievement in demonstrating the biexciton Rabi oscillation is that the π pulse served as the operational pulse of a CROT gate. To be more specific, the operational pulse for

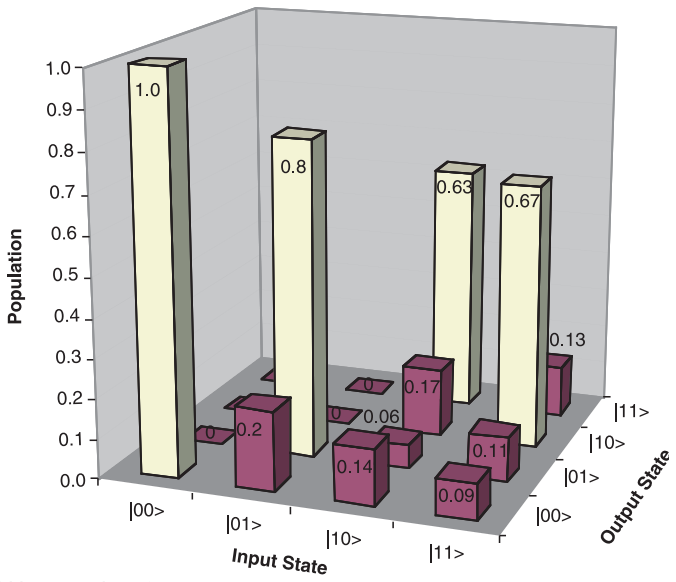

Fig. 4. Truth table of the numerically simulated CROT gate. Like the truth table of a classical gate, it records the population rather than the probability amplitude in each state at the output that corresponds to a particular input state. For example, column 3 indicates that the populations in states $|00\rangle$, $|01\rangle$, $|10\rangle$, and $|11\rangle$ are 0.14, 0.06, 0.17, and 0.63, respectively, after the CROT operation, assuming that the system starts in state $|10\rangle$. In an ideal gate, the four highest bars would have a value of 1 and the others would have a value of 0.

the CROT gate was chosen to be a π pulse tuned to the $|10\rangle \leftrightarrow |11\rangle$ transition. If the input of the gate is $|00\rangle$, the operational pulse will be off-resonant and the output will remain $|00\rangle$. If the input is $|01\rangle$, the operational pulse will have the wrong polarization and the output will not change, as verified experimentally (*16*). However, when the input is $|10\rangle$, the operational pulse rotates the input to $-|11\rangle$. Similarly, if the input is chosen to be $|11\rangle$, the operational pulse stimulates it down to $|10\rangle$. Thus, the truth table of the CROT was mapped out with a π pulse tuned to the $|10\rangle \leftrightarrow |11\rangle$ transition.

This description of the gate operation assumes that the optical coupling is ideal, which leads to complete Rabi oscillations. In reality, quantum systems couple to their environment (e.g., phonons and vacuum fluctuations), causing pseudo-spin relaxation and dephasing, i.e., decoherence, which prevent complete Rabi oscillations.

Although this system is only a model to demonstrate the potential for coherent, optically driven quantum computing in scalable architectures based on multidot systems, it is useful to quantify the performance and evaluate the impact of the operating parameters. To do that, we compared the ideal truth table with the physical truth table (Fig. 4) calculated on the basis of experimentally determined parameters (supporting online text). It is important to recognize that the rotation of the $|00\rangle$ state to either the $|01\rangle$ or $|10\rangle$ state was calculated to be 0.80, in excellent agreement with the measured value of 0.77 ± 0.06.

It is possible to define a simple parameter that describes the performance of the CROT gate to facilitate comparison between different implementations. The gate fidelity, $\overline{|\langle\psi|U_P^\dagger U_I|\psi\rangle|^2}$ where ψ is the wave function, U_I is the ideal unitary transformation matrix, and $U_P^\dagger$ is the complex conjugate of the physical unitary transformation matrix, first defined in (*18*), is one such parameter. The definition can be naturally extended to $F = Tr[\rho_P(t)\rho_I(t)]$ to take dephasing into account, where $\rho_P(t)$ and $\rho_I(t)$ are the physical and ideal density matrices after the gate operation, F is the gate fidelity, and Tr represents the trace. The overline indicates an equally weighted average over all possible initial states of the four-level system. An ideal gate would have fidelity of 1, whereas any real gate would have fidelity between 0 and 1. The fidelity of the current CROT gate is calculated to be 0.7 (supporting online text).

Long operational pulses and short dephasing times due to fast recombination, a consequence of the large dipole moment, are two key issues that lead to the fidelity below 1 of the current gate. Long pulses (5 ps) were used in our experiments in order to avoid exciting multiple excitons under the same aperture. Using a smaller aperture or a different sample with more isolated excitons will enable us to use shorter pulses. A much more versatile and efficient solution is to use the technique of pulse shaping (*4*). Much longer recombination and dephasing times, on the order of several hundred picoseconds, have been reported (supporting online text) in self-assembled QDs (*19–21*). The combination of a short operational pulse (1 ps) and long population-relaxation times (200 ps) with no pure dephasing would lead to a much improved gate, with fidelity as high as 0.97 with the optimal separation between pulses.

The interacting two-exciton system studied here is formed by two excitons in the same QD. Although this system is the simplest model system for the study of a two-bit gate, it is not really scalable by adding an arbitrary number of excitons into a dot, where qubits are based on dipole transitions with relatively short lifetimes. A variety of schemes exist for scalable quantum computers based on semiconductor QDs, such as the QD-microcavity systems (*22*), QDs attached to a linear support (*23*), and doped QDs coupled through exchange interactions (*10*). An essential element of these proposals is the introduction of a controllable coupling between qubits. In the work of Piermarocchi *et al*. (*10*), qubits were represented by spin degrees of freedom of the electrons localized in a patterned array of doped self-assembled QDs. Although our present work relies on creating a real population of two interacting excitons, optical manipulation of spin through virtual excitons can be realized in the adiabatic limit and is robust against decoherence through population relaxation. The recent studies demonstrating long-lived spin coherence in semiconductors (*24*), coupled with the rapid pace of advances in quantum dot fabrication, make proposals based on manipulation of spins attractive.

References and Notes

1. A. Barenco, D. Deutsch, A. Ekert, R. Jozsa, *Phys. Rev. Lett.* **74**, 4083 (1995).
2. F. Troiani, U. Hohenester, E. Molinari, *Phys. Rev. B* **62**, R2263 (2000).
3. E. Biolatti, R. C. Iotti, P. Zanardi, F. Rossi, *Phys. Rev. Lett.* **85**, 5647 (2000).
4. P. Chen, C. Piermarocchi, L. J. Sham, *Phys. Rev. Lett.* **87**, 067401 (2001).
5. F. de Martini, V. Bužek, F. Sciarrino, C. Sias, *Nature* **419**, 815 (2002).
6. T. H. Stievater *et al.*, *Phys. Rev. Lett.* **87**, 133603 (2001).
7. H. Kamada, H. Gotoh, J. Temmyo, T. Takagahara, H. Ando, *Phys. Rev. Lett.* **87**, 246401 (2001).
8. H. Htoon *et al.*, *Phys. Rev. Lett.* **88**, 087401 (2002).
9. A. Zrenner *et al.*, *Nature* **418**, 612 (2002).
10. C. Piermarocchi, P. Chen, L. J. Sham, *Phys. Rev. Lett.* **89**, 167402 (2002).
11. G. Burkard, D. Loss, D. P. Divincenzo, *Phys. Rev. B* **59**, 2070 (1999).
12. D. Gammon, E. S. Snow, B. V. Shanabrook, D. S. Katzer, D. Park, *Science* **273**, 87 (1996).
13. K. Brunner, G. Abstreiter, G. Böhn, G. Tränkle, G. Weimann, *Phys. Rev. Lett.* **73**, 1138 (1994).
14. D. Gammon, E. S. Snow, B. V. Shanabrook, D. S. Katzer, D. Park, *Phys. Rev. Lett.* **76**, 3005 (1996).
15. G. Chen *et al.*, *Phys. Rev. Lett.* **88**, 117901 (2002).
16. T. H. Stievater *et al.*, *Phys. Rev. B* **65**, 205319 (2002).
17. J. R. Guest *et al.*, *Phys. Rev. B* **65**, R241310 (2002).
18. J. F. Poyatos, J. I. Cirac, P. Zoller, *Phys. Rev. Lett.* **78**, 390 (1997).
19. P. Borri *et al.*, *Phys. Rev. Lett.* **87**, 157401 (2001).
20. D. Birkedal, K. Leosson, J. M. Hvam, *Phys. Rev. Lett.* **87**, 227401 (2001).
21. M. Bayer, A. Forchel, *Phys. Rev. B* **65**, R041308 (2002).
22. A. Imamoğlu *et al.*, *Phys. Rev. Lett.* **83**, 4204 (1999).
23. K. R. Brown, D. A. Lidar, K. B. Whaley, *Phys. Rev. A* **65**, 012307 (2001).
24. J. M. Kikkawa, D. D. Awschalom, *Phys. Rev. Lett.* **80**, 4313 (1998).

25. Supported in part by the Office of Naval Research, the National Security Agency, and Advanced Research and Development Activity under the Army Research Office (contract nos. DAAG55-98-1-0373 and DAAD19-01-1-0478); the Air Force Office of Scientific Research (grant no. F49620-99-1-0045); the National Science Foundation (grant no. DMR 0099572 and FOCUS); and the Defense Advanced Research Projects Agency/Spins. D.G.S. thanks the Guggenheim Foundation for their support.

Supporting Online Material

www.sciencemag.org/cgi/content/full/301/5634/809/DC1
SOM Text
References and Notes

24 February 2003; accepted 25 June 2003